Bulletin of Earth Sciences of Thailand

A new mangrove core record for Eastern Thailand: chemical characterization of bulk organic sediment by FTIR–ATR spectroscopy and elemental analysis

Naomi Seaton[1], Sakonvan Chawchai[1], Prompong Pienpinijtham[2]
Ludvig Löwemark[3]
[1] Department of Geology, Faculty of Science, Chulalongkorn University, Bangkok 10330, Thailand
[2] Department of Chemistry, Faculty of Science, Chulalongkorn University, Bangkok 10330, Thailand
[3]Department of Geosciences, National Taiwan University, Taipei City 10617, Taiwan (R.O.C.)

Abstract

The eastern Gulf of Thailand features mixed low-relief geomorphology, characterized by intertidal mudflats, coastal wetlands, and relict sand deposits indicative of prograding barrier systems formed during Holocene regression. While previous research has focused on reconstructing sea-level changes using beach ridge records and mangrove pollen, there has been no comprehensive investigation into organic geochemical archives. This work aims to provide a new mangrove core record for Eastern Thailand, focused on chemical characterization of organic sediments and proxy reconstructions of relative environmental changes with depth, complementary to growing literature on coastal paleoenvironmental change in this region of the Gulf of Thailand. This research adopts an innovative approach to reconstructing environmental change by analyzing the chemical composition, relative sources, and cycling dynamics of mangrove organic matter, employing loss-on-ignition (LOI), elemental analyses, and Fourier-transform infrared (FT-IR) spectroscopy techniques. The PEM stratigraphic units encompass nutrient-poor surface tidal wash, organic-rich mangrove soils with active humus formation, and basal shallow marine sands with low organic content and high-energy horizons of fragmentary shells. Enhanced organic decomposition is evident in bioturbated surface sediments, while high total organic carbon to total nitrogen (TOC/TN) ratios indicate substantial allochthonous contributions from mangrove leaf litter and detrital organic matter via runoff from the Prasae River. Fluctuating TOC/TN values and FT-IR absorbances at 2925–2905 cm^{-1} and 3300 cm^{-1} reflect significant mixing between terrestrial and aquatic organic matter, linked to dynamic sea-level changes and increasing riverine inputs. The organic mangrove soils exhibit FT-IR absorption peaks for phenolic and aromatic compounds at 1630 cm^{-1}, indicating advanced humification stages, while the basal sands preserve higher proportions of aliphatic hydrocarbons, as indicated by vibrations at 1475 cm^{-1}, suggesting influences from grain size, sulfur-reduction pathways, and the inhibitory effects of high phenolic content on organic carbon preservation.

Keywords: Tropical Mangrove, Coastal Wetland, FT-IR Spectroscopy, Elemental Analysis, Organic Geochemistry

1. Introduction

1.1 Mangrove systems and sedimentation

Mangrove forests are tidal wetland systems that occupy an estimated 75% of the global coastline, the majority of which is restricted to tropical and subtropical zones (Alongi, 2014). In 2020, there was an estimated 145,068 km^2 of mangrove coverage globally, nearly 40% of which could be found in Asia (Jia et al., 2023). These coastal ecosystems are regarded among the most productive environments on Earth and represent important ecological and economic resources. Mangroves provide essential natural services in the form of protection from storm surges and coastal erosion, sediment catchment, biogeochemical cycling, and

carbon capture, a source of renewable timber, a crucial habitat for coastal biodiversity, and critical nurseries that sustain commercial fisheries (Pernetta, 1993; Yulianto et al., 2004; Twilley and Day, 2012; Shiau and Chiu, 2020; Zhu and Yan, 2022).

Mangroves are also recognized as major blue carbon sinks that draw down carbon at much higher rates per unit area than all other terrestrial ecosystems, excluding peatlands and tundra (Mcleod et al., 2011; Alongi, 2014; Zhu and Yan, 2022). Global mangrove carbon sequestration has been variously estimated between 8.6–25 Tg a^{-1} (Twilley et al., 1992; Duarte et al., 2005; Alongi, 2018), accounting for less than 7% of total terrestrial carbon stocks but nearly 20% of all stored organic carbon in tropical marine settings (Alongi, 2020) by the combined pathways of photosynthetic carbon fixation and *in situ* soil formation where decomposed organic matter (OM) is converted into humic substances, recalcitrant carbon-bearing compounds, or adsorbed by siliclastic minerals that stabilize soil organic carbon (Chmura et al., 2003; Twilley and Day, 2012).

Plant species distribution is controlled by variations in the stress conditions that influence vegetative growth, such as salinity gradients, differences in soil pH, and the hydroperiod (Twilley and Day, 2012). Salt tolerance is highly variable among mangrove species (Hossain and Nuruddin, 2016; Woodroffe, 2018; Worthington et al., 2020), resulting in zoned growth dominated by characteristic genera as a result of natural ecological succession in response to sediment accretion and mangrove colonization over prograding substrates. As conditions shift, so too does the plant distribution. This environmental sensitivity and fast-paced ecological response make mangroves valuable records of coastal paleoenvironmental dynamics (Woodroffe, 2018).

Due to differences in plant chemical compositions between mangrove species, it is hypothesized that variable primary leaf litter chemistry may also preserve unique geochemical signatures during soil formation. On the other hand, adaptive differences in root morphology will invariably influence modes of sediment trapping and substrate development. Therefore, decoding the chemical profile of mangrove sediments can help elucidate relative environmental changes and provide insight into the provenance or processes that formed those sedimentary records.

1.2 Mangrove soil formation

Mangrove soil formation is a complex process influenced by the unique coastal environment where these trees grow. Tidal fluctuations create waterlogged conditions that promote anaerobic decomposition of organic matter, such as fallen leaves and plant roots. Microbial activity, including bacteria and fungi, breaks down this material, producing bioavailable nutrients and organic acids. In tropical settings, warmer temperatures may accelerate this process, though plant lignins and the woody components of vascular plants are more resistant to decomposition, leading to the accumulation of partially decayed matter that is further transformed into humic substances (HS) during 'humification,' defined as the degradation or alteration of organic material in soils and composts resulting in the formation of humus (Hayes and Swift, 2020) that can be further fractionated into humic acids, fulvic acids, and humans (Nardi et al., 2021), HS are characterized by organic functional groups such as carboxylic acid, phenolic and alcoholic hydroxyls, ketone, and quinone groups (Gaffney et al., 1996; Fenchel et al., 2012) so mature soils in advanced stages of humification are measurably enriched in these moieties.

1.3 FT-IR spectroscopy in characterizing mangrove organic matter

Many studies have attempted geochemical characterizations of tropical coastal sediments (e.g., Zhang et al., 2011; Matthew et al., 2021;

Senanayake et al., 2021), focused on constraining the sources of OM in mangrove soil or producing a qualitative soil profile using elemental and spectroscopic techniques. Fourier-transform infrared spectroscopy (FT-IR) is a rapid, non-destructive method of identifying reactive functional moieties in bulk sediment samples. In this work, attenuated total reflectance FT-IR is employed to identify key organic functional groups representative of major components found in organic soils. FT-IR ATR absorptions at 1060 cm^{-1} (polysaccharide C–O stretch), 1160 cm^{-1} (phenolic C–O), and 1630 cm^{-1} (aromatic C=C and carboxylates) can be used to determine relative changes in humification with depth by comparing the peak height proportions of recalcitrant moieties, typically enriched in degraded soils, with polysaccharide functional groups indicative of labile substances like cellulose and hemicellulose found in bulk organic sediment (Niemeyer et al., 1992; Broder et al., 2012; Senanayake et al., 2021; Obeng et al., 2023).

1.4 Study site and geological setting

The Prasae Estuary Mangrove (PEM) is an estuarine fringing mangrove located at the mouth of the Prasae River in Pak Nam Prasae, Klaeng District, Rayong Province, Eastern Thailand (Figure 2A). Under the jurisdiction of the Thai Department of Marine and Coastal Resources, the present–day mangrove holds protected status as a national forest. It is famous for the 'Thung Prong Thong' or 'Golden Meadow,' an open mangrove meadow dominated by various species of *Ceriops* that also serves as a popular ecotourism destination in Rayong Province. As such, an elevated boardwalk provides convenient access to the western limit of the PEM for visitors to Thung Prong Thong, while boat–access through tidal creeks into the mangrove interior is possible.

Coastal geomorphic mapping by the Thai Department of Mineral Resources in 2001 interpreted the Prasae Estuary and mangrove forest to host mixed geomorphology dominated by intertidal mudflats and old sand or beach deposits, as well as areas significantly disturbed areas by intensive shrimp farming and land use change.

From satellite imagery (Google Earth, 2022) and field surveys, three distinctive vegetative zones are observed in the PEM. The shore–parallel vegetative bands develop successively landward, exhibiting sharp delineations between each zone. By ecological classification, the intermediate mangrove in the PEM is characterized by *Ceriops* and *Rhizophora* species, split into two zones for this study, while *Avicennia* and *Sonneratia* species dominate the dynamic shoreface (Figure 2C).

Sedimentation mode in the PEM is mixed but predominantly allochthonous, especially in the seaward zone. There are two main influences on deposition: 1) fluvial dynamics related to the Prasae River estuary, where terrigenous sediments are delivered via long-shore drift, and 2) the trapping of higher–energy marine clastics in sediment weirs created by entangled mangrove roots during tidal inundation or wave action (Scholl, 1997; Woodroffe, 1992). The present-day mangrove is sheltered from wave–action behind a growing barrier beach or sand bar, emerging from a combination of fluvial transport and deposition on the Prasae River mouth, longshore drift, and tidal transport. This geomorphology is consistent with models of the composite river and wave-dominated mangrove development (Woodroffe, 1992), where a wetland system may emerge in the low–energy back-barrier environment of a prograding barrier system and sediment supply is delivered tidally (Slatt, 2013).

According to updated Köppen–Geiger climate maps (Beck et al., 2018), modern-day Prasae experiences a tropical savanna climate (Aw) and lies on the boundary with a zone of tropical monsoon climate to the east in neighboring Chanthaburi Province. Paleoenvironmental reconstructions from lake and coastal sediments indicate transitions to wetter conditions in northeastern Thailand from the Younger Dryas to the mid–Holocene (Chabangborn, 2017) while

analysis of sedimentary features along the Chanthaburi estuary, near the study site for this work, interpreted evidence for increased freshwater input indicative of wetter climatic conditions during the late Holocene (Ballian et al., 2023). Therefore, it is possible that local hydrology, influenced by monsoon seasonality and temporal shifts in the Intertropical Convergence Zone (ITCZ), will significantly vary the degree of terrigenous material supplied from surface runoff and fluvial discharge (Scholl, 1997), reflected in the geochemistry of mangrove soils. Towards the inland interior of the PEM, leaf litter and subsurface root complexes associated with *Ceriops* and *Rhizophora* support rapid sediment accretion and the *in-situ* development of organic soils and peat. As a result, the mode of sedimentation is expected to match differences in root morphology and ecological zonation, trapping predominantly allochthonous clastic inputs near the shore to more autochthonous or mixed signals towards inland transitional zones.

Previous lithofacies studies of Rayong and Chanthaburi province coastlines, including Prasae in Klaeng District, identified the presence of estuarine mudflats, prograded barrier sands, transgressive erosional lag sands, relict strandlines, and littoral mudflats (Choowong, 2002), concluded evidence for a transitional marine lithofacies with distinctive features of sea-level regression.

The sea-level envelope has been well documented for the Gulf of Thailand and the Thai–Malay peninsula (Figure 1), suggesting gradual regression following a mid–Holocene highstand in this region. Parallel beach ridge deposits up to 5 km inland are commonly present along Thailand's Eastern seaboard from Rayong to Trat province (Choowong, 2002; Ballian et al., 2023), which appears to support this regional interpretation.

However, high-resolution pollen-based reconstructions using island mangrove sedimentary records at high resolution (Englong et al., 2019) have painted a more dynamic portrait of sea-level history in Eastern Thailand during the late Holocene, suggesting highly variable sea-level fluctuations between 1500–1300 cal yr BP, followed by progressive transgression between 1300–500 cal yr BP, and progressive regression over the last 500 years.

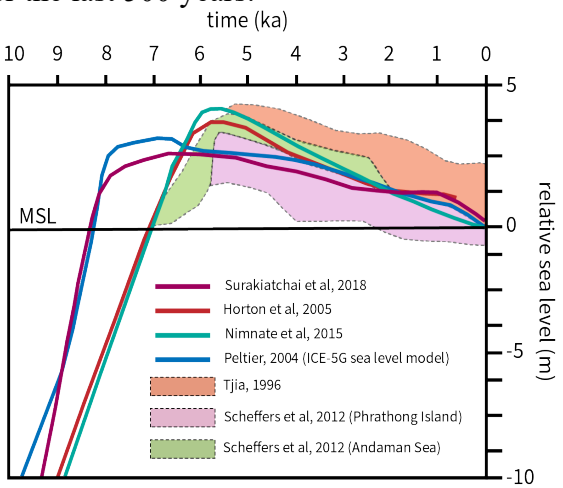

Figure 1. Sea-level envelope for the Gulf of Thailand and the Thai-Malay peninsula, modified after Miocic et al. (2022)

Sedimentary records of coastal paleoenvironments and paleoclimate remain sparse for Eastern Thailand. Recently, studies have focused on reconstructing sea-level changes using beach ridge records (e.g., Ballian et al., 2023) and mangrove pollen (Englong et al., 2019), but few have reported on the dynamics of organic mangrove soil formation or geochemical proxies for decomposition processes that also record shifts in mangrove sediment input and ecological responses to environmental change. It is necessary to note that intensive economic activity, particularly industrialized shrimp farming, and manufacturing along Thailand's Eastern seaboard, including in Pak Nam Prasae, has led to a rapid decline in mangrove cover and, as yet, an unquantified impact from anthropogenic pollutants. Around the study site, shrimp farming is concentrated to the north, approximately 1 km inland of the present–day shoreline.

This work aims to provide a new mangrove core record for Eastern Thailand, focused on chemical characterization of organic sediments and proxy reconstructions of relative

environmental changes with depth, complementary to growing literature on this region of the Gulf of Thailand.

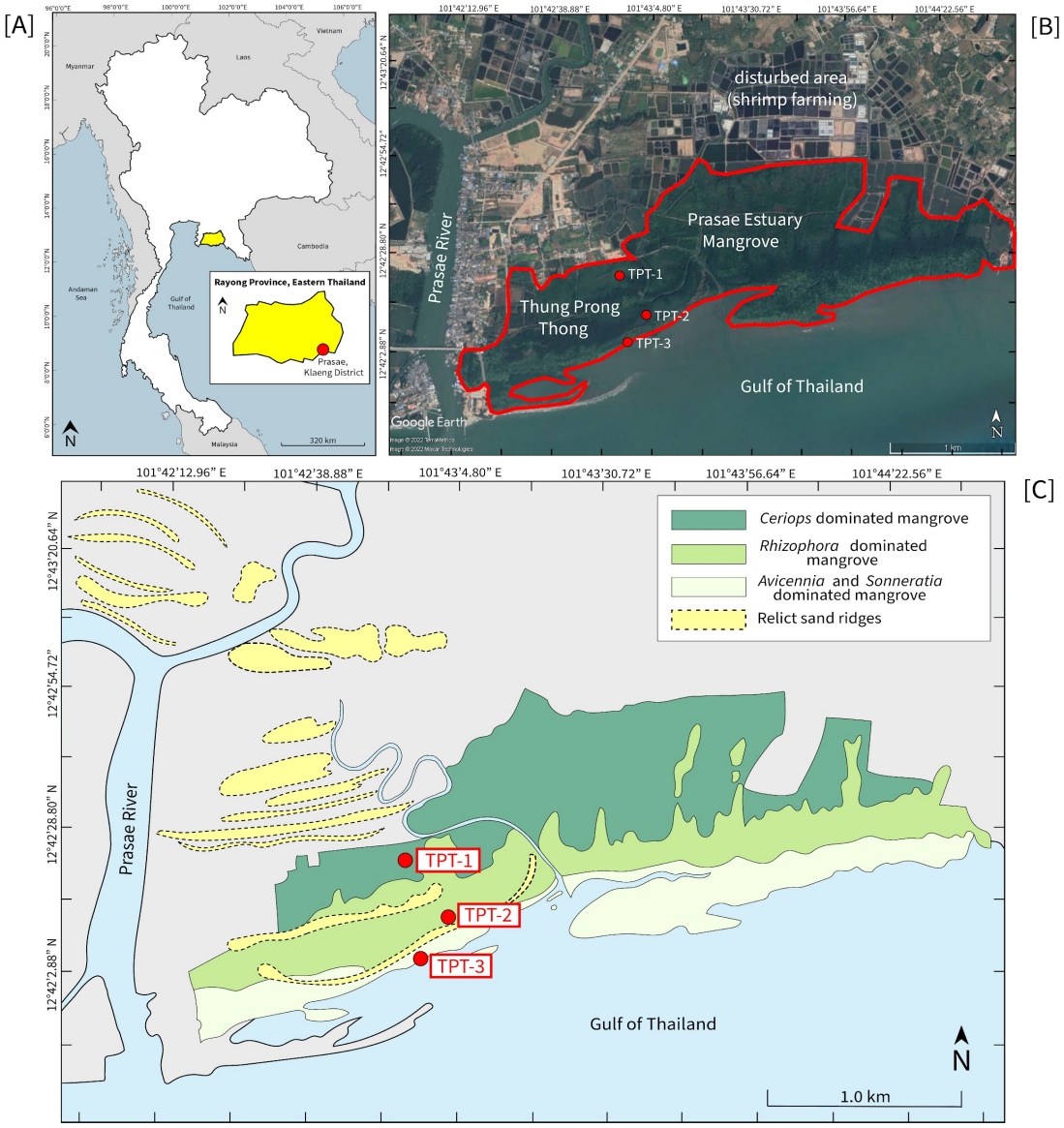

Figure 2. (**A**) Study area (red marker) location in Rayong Province, Eastern Thailand (**B**) 1:150,000 scale satellite map (Google Earth, 2022) of the Prasae Estuary Mangrove (**C**) Schematic map of interpreted ecological zonation in the Prasae Estuary Mangrove system with TPT coring sites marked in red.

2. Methodology

2.1 Site survey

Differential GPS measurements were recorded on a 650 m transect from the inland mangrove locality at TPT-1 (12.706348, 101.715689) to the seaward mangrove locality at TPT-3 (12.701503, 101.716088), along the route of a publicly accessible boardwalk, to map low–relief topographical features in the mangrove forest interior. A vegetation survey was also conducted along the transect and compared against

observations from satellite imagery (Google Earth, 2024) to constrain the spatial distribution of mangrove vegetative zones.

2.2 Sample collection and preparation

One sediment core was collected per coring site to sample three distinctive vegetative zones inside the PEM. To minimize obstructions and damage to both mangrove roots and coring equipment, gouge corers were used to test suitable areas before the core was recovered using an 8 cm diameter Russian corer. TPT-1 (190 cm) and TPT-2 (184 cm) were sampled using a Russian corer due to the muddy, organic-rich nature of surface mangrove sediment. TPT-3 (178 cm) was sampled with a 3 cm diameter gouge corer instead to penetrate tightly compacted, coarse-grained sand deposited at the seaward mangrove zone. The maximum depth of each core varies due to the limitations of coring through densely rooted surface sediments or tightly compacted waterlogged sand.

Scaled photographs and stratigraphic descriptions were taken before subsampling at 1 cm resolution on site. Sub-samples were then sealed and refrigerated (<5◦C) to limit decomposition by biological activity until further treatment.

Samples at 4 cm intervals from each core were selected for bulk sediment geochemical analysis. Half of each selected sample was freeze-dried and ground into fine powder. The remaining halves were stored as wet samples under refrigeration.

2.3 Loss-on-ignition analysis

Loss-on-ignition tests were conducted at the Department of Geology at Chulalongkorn University, Bangkok, Thailand, on wet samples at 4 cm resolution for each core, beginning at 0 cm core depth to represent the modern–day mangrove surface. Forty-seven samples were selected from TPT-1, 44 samples from TPT-2, and 42 samples from TPT-3. Each wet sample was halved by mass (25% mass of original sub-sample) and oven–dried at 105◦C for 12 hours. For TPT-1, 0.200g of dried sample was used for analysis due to the limited mass of the initial wet sample; for TPT-2 and TPT-3, 1.000g of dried sample was measured into each crucible. Combustion in a muffle furnace was conducted at 550◦C for 5 hours and at 950◦C for 3 hours to measure $LOI_{550◦C}$ (organic content by wt%) and $LOI_{950◦C}$ (carbonate content by wt%), respectively.

All post-combustion masses were recorded after leaving hot crucibles to cool for 1 hour at room temperature.

2.4 Elemental analysis

Powdered freeze-dried samples were pre-treated at the Department of Geology, Chulalongkorn University. Samples were mixed with 5 ml 2M HCl solution and left to react for 18 hours to remove inorganic carbonate. After 18 hours, an excess of 2M HCl was added to samples and agitated until effervescence ceased completely. Acid–treated samples were washed with distilled water until pH–pH-balanced and oven–dried at 40◦C for 72 hours. 15–20 mg of each pre-treated sample was then wrapped in pressed tin capsules for elemental analysis, conducted with an Elementar Vario MICRO Cube at the Institute of Oceanography, National Taiwan University (IONTU), for total organic carbon (TOC%) and total nitrogen (TN%), calibrated against peaty and sandy soil standards (LECO 502–309 and LECO 502–062, lot: 1018 respectively).

2.5 Fourier-transform infrared spectroscopy

FT-IR ATR measurements were conducted at the Department of Chemistry at Chulalongkorn University, Bangkok, Thailand. Bulk sediment FT-IR ATR spectra were collected at 4 cm^{-1} resolution, using 64-scan averages on a ThermoScientific Nicolet iS5 FTIR spectrometer with iD7 ATR diamond attachment for 36 representative samples from the near-surface mangrove soil and underlying sands of all three mangrove sediment cores to compare compositional variation between each stratum. Spectra were acquired in the 4000–400 cm^{-1} range.

Freeze-dried samples were hand–ground to homogenous powder with an agate mortar and pestle. Ground samples were transferred directly onto an ATR diamond attachment, and the swivel pressure tower was hand–adjusted to ensure generous contact between powdered samples and the ATR attachment.

FTIR–ATR spectra were collated and analyzed using OMNIC™ for Dispersive Raman software. Second derivative spectra were obtained to identify the peak positions with more clarity, mitigating inaccuracies associated with interpreting noisy bulk sediment spectra.

2.6 Peak height ratios: humification and the degree of decomposition

Two humification indices were calculated after (Senanayake et al., 2021) and (Obeng et al., 2023) using peak height ratios obtained from FT-IR ATR spectra for TPT core samples.

To compare recalcitrant phenolic (1160 cm^{-1}) and aromatic (1630 cm^{-1}) moieties, typically enriched in degraded soils, the peak height ratios at 1160 cm^{-1} and 1630 cm^{-1} were determined by dividing recorded absorption intensities at these positions with the peak height at 1060 cm^{-1} in the same sample that represents the C–O stretching of labile polysaccharides, presented as I_{1160}/I_{1060} and $I_{1630}/I_{1060.}$, respectively.

Decomposition with depth is quantified by the ratio $I_{1060}/I_{3300,}$ which compares the absorption intensity of polysaccharide C–O stretching with the peak height of vibrations at 3300 $cm^{-1,}$ which represents O–H alcohol stretching.

Peak heights were taken from the intensity values recorded at specific peak positions for phenolic, aromatic, and polysaccharide functional groups identified in second derivative FT-IR spectra using the built-in peak height tool in OMNIC™ software for Dispersive Raman. This method allowed for more reliable manual placement of baselines and discernment of peak position in noisy bulk sediment spectra.

3. Results

3.1 Transect cross-section

Elevation ranges between 0–1.6 m above mean sea level along a 2 km transect perpendicular to the modern shoreline (Figure 3). Two elevated ridges were identified inside the mangrove complex between the three coring points. To the north, the area is disturbed by intensive shrimp farming and land–use, preventing access and accurate measurements with D–-GPS.

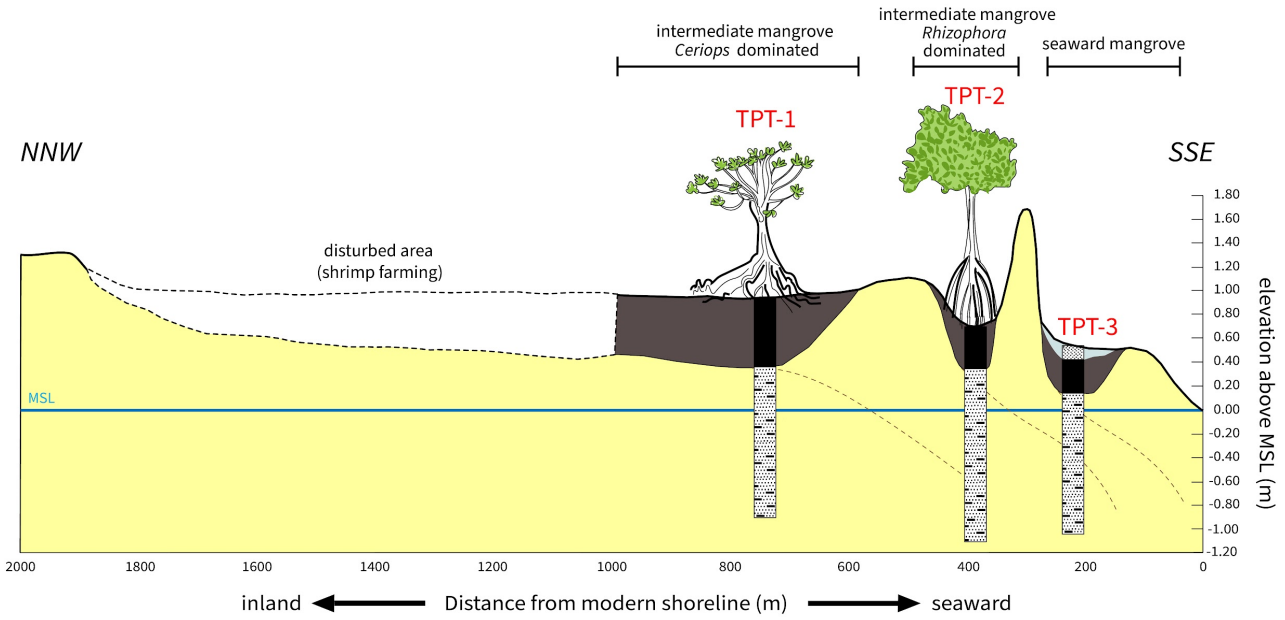

Figure 3. Cross–section elevation profile of the Prasae Estuary Mangrove constructed from D–GPS measurements.

3.2 Core stratigraphy

Three distinguishing strata were identified in the TPT mangrove cores: an upper coarse sand, organic-rich mangrove soil, and an underlying layer of bioclastic muddy sand characterized by white horizons of fragmented shells (Figure 4). Stratigraphic thicknesses vary between each locality.

TPT-1 and TPT-2 cores show heavily bioturbated mangrove soil at the surface, 0–60 cm and 0–40 cm thickness, respectively, characterized by brown–black coloration from high organic content and a fine-grained matrix of silts and sands. Surface sediments are mixed by both modern epifaunal activity and bioturbated at depth by a dense network of mangrove plant roots.

At the TPT-1 locality, present-day *Ceriops* roots (~3 cm width) and extensive entanglements of fine, fibrous rootlets are present throughout the mangrove soil. At TPT-2, the mangrove soil is disturbed by thick, woody *Rhizophora* tap roots and stilted, subaerial roots that extend vertically through a soft substrate up to 20 cm in the core. An abrupt contact is noted in the TPT-1 and TPT-2 cores, at 60 cm and 101 cm, respectively, transitioning to a thick lower unit of lighter gray, fine–medium muddy sand punctuated at intervals by thin layers of poorly sorted, fragmentary bioclasts (~1–4 mm width). Some intact shells in these high–energy horizons suggest a mixture of small bivalves and other broken mollusk material.

At TPT-3, all three stratigraphic units are observed (Figure 4C). Coarse sand (0–16cm) overlies a relatively thin unit of organic mangrove soil (16–42cm), and the same bioclastic muddy sand is observed at the base of TPT-1 and TPT-2 cores. Coarse surface sand is compact and bioturbated by pneumatophores (aerial roots) typical of *Avicennia* and other colonizing mangrove species on the shoreface.

3.3 Loss-on-ignition

Organic matter (OM), measured as $LOI_{550°C}$ wt%, fluctuates with depth in all cores. Overall, OM generally decreases with depth.

TPT-1 recorded the highest OM (Figure 4A): 45.50 wt% at the modern mangrove surface and an average of 25.43 wt% in the upper 56 cm compared to 3.02 wt% in the lower 134 cm. TPT-2 (Figure 4B) recorded 5–15 wt%, and TPT-3 displayed the lowest average OM at 1–14 wt%. $LOI_{550°C}$ patterns for TPT-3 (Figure 4C) differ from TPT-1 and TPT-2, showing low OM at the core surface (0–30 cm) and an OM peak between 30–44 cm core depth before decreasing again with depth. Carbonate content also fluctuated but was low for all samples at under 5% by weight at every locality. $LOI_{950°C}$ values reflect relatively constant carbon content and appear unaffected by changes in depth.

Loss-on-ignition analysis shows a sharp decline in OM between organic-rich surface sediments and calcareous muddy sands below, consistent with stratigraphic observations made for all three cores.

3.4 Total carbon and nitrogen

Total nitrogen (%TN) and total organic carbon (%TOC) in all three cores (TPT-1, TPT-2, TPT-3) are coherent, showing excursions consistent with three separate stratigraphic units. In general, %TN and %TOC are highest in the upper 60 cm of TPT-1, the upper 40 cm of TPT-2, and in two horizons of TPT-3, between 20–40 cm and around 90cm depth, which coincides with the observed stratigraphic occurrence of organic-rich mangrove peat horizons (Figure 4). In general, %TOC and %TN decrease with depth. TPT-1 exhibited the highest %TOC at up to 10% by mass, followed by TPT-2 at up to 5.5%. TPT-3 showed notably low organic carbon content, recording a maximum of 1.85% TOC at 36–37 cm core depth. For all cores, organic carbon remained at less than 2% by mass below 60 cm for TPT-1 and below 40 cm for TPT-2 and TPT-3, closely mirroring loss-on-ignition trends.

Carbon largely arises from vascular plant material, characterized by carbon-rich and nitrogen–depleted lignin and cellulosic components, while protein-rich aquatic algae provide a significant natural source of nitrogen

(Bianchi and Canuel, 2011; Kumar et al., 2018; Carneiro et al., 2021), TOC/TN is a useful proxy for identifying the relative sources of chemical components in organic soils.

The TOC/TN ratio in the TPT mangrove cores ranged from 2.56 to 52.76. In general, the cores exhibited relatively high mean TOC/TN with values that broadly decreased with depth (Figure 4). TPT-1 showed 22.84 average TOC/TN, subdivided into TOC/TN = 30.21 at the 0–128 cm depth range compared to 9.95 in the 128–188 cm range. TPT-2 exhibits 22.26 average TOC/TN, separated into TOC/TN = 26.64 in the 0–128 cm depth range compared to 11.66 for 128–172 cm. In contrast, TPT-3 recorded depressed TOC/TN values compared to the other two inland localities, showing a whole–core mean TOC/TN of 18.15: 6.19 for 0–16 cm, 24.95 for 20–52 cm, and 18.40 at the 56–164 cm depth range.

Linear regressions for TOC% plotted against TN% produced R–values > 0.8, where TPT-1 (R^2 = 0.976), TPT-2 (R^2 = 0.935), and TPT-3 (R^2 = 0.818) supported a strong positive correlation between total organic carbon and measure total nitrogen.

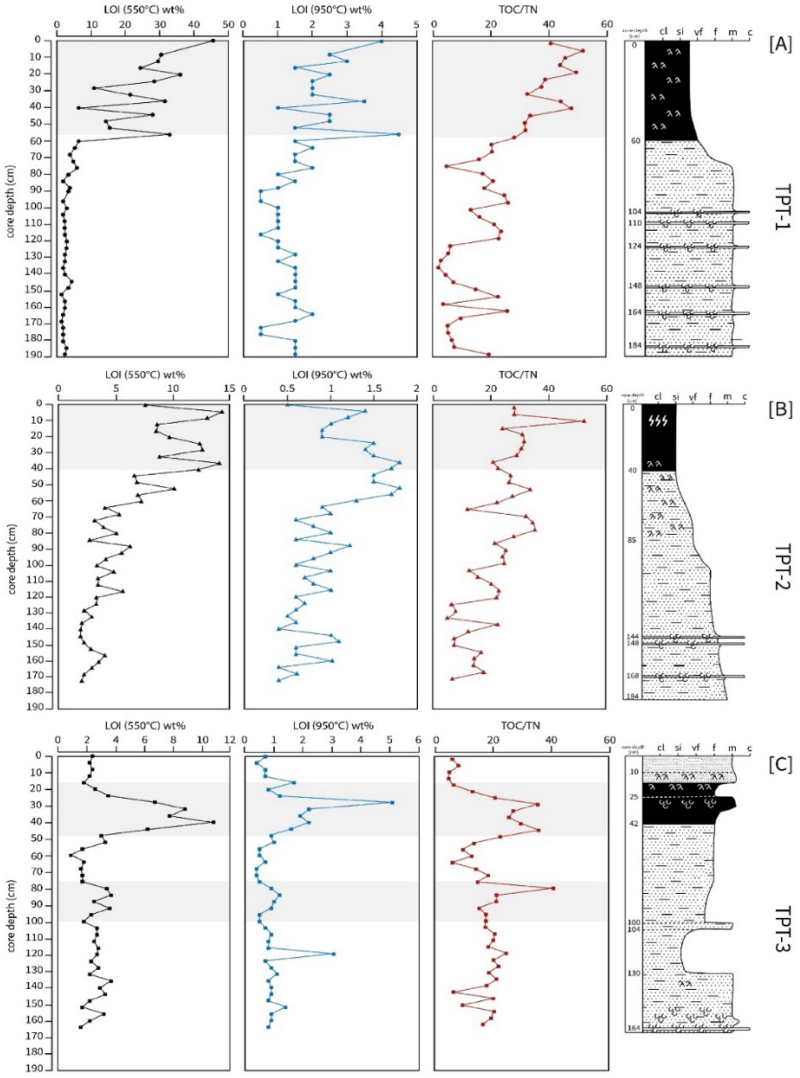

Figure 4. Loss-on-ignition results for combustion at 550°C (organic matter wt%) and 950°C (carbonate content wt%), TOC/TN ratios with depth, and stratigraphic sections for TPT-1 (**A**), TPT-2 (**B**), and TPT-3 (**C**).

3.5 Fourier-transform infrared spectroscopy

Only absorptions observed between 1800–400 cm^{-1} were interpreted for this study, owing to a relative featurelessness in the diagnostic region (4000–1800 cm^{-1}). A weak absorption band occurring around 3300 cm^{-1} is noted in all samples, attributed to H–bonded O–H stretching or possible trace N–H stretching (Gaffney et al., 1996; Socrates, 2004; Zhang et al., 2011). Two peaks at 2925–2905 cm^{-1} and 2855–2840 cm^{-1} are also recorded in all samples, corresponding to asymmetric and symmetric C–H stretching of aliphatic groups or the presence of aldehydes in 2 bands (Gaffney et al., 1996; Gonzalez–Perez et al., 2008; Barreto et al., 2016).

Absorption peaks at 1170–1150 cm^{-1}, 1045–1018 cm^{-1}, 1015–990 cm^{-1}, 930–900 cm^{-1}, 805–786 cm^{-1}, 780–765 cm^{-1}, 700–685 cm^{-1}, and 542–516 cm^{-1} appear in every core at all relative depths, denoting the presence of silica–related groups, C–O polysaccharide stretching, and C–O ester/ether/phenol stretching attributable to lipid–like components. Observed absorption bands in the PEM and their functional assignments are summarized in Table 1.

Sediments from all three core locations exhibit similar spectra, consistent with observations of the same three stratigraphic units present in the PEM system, with obvious physical and chemical transitions at depths supported by the results of LOI and TOC/TN analyses. The FT-IR spectra also support these distinctive chemical shifts with depth as certain reactive function groups appear to distinguish upper organic mangrove peat units from lower bioclastic muddy sands (Figure 5).

TPT-1 and TPT-2 feature single, high-intensity absorption bands near 1600 cm^{-1}, centered around 1640 cm^{-1}, in all surface organic mangrove peat samples (0–56 cm of TPT-1 and 0–45 cm of TPT-2). This peak is notably missing from the upper 40 cm of core TPT-3, including coarse surface sands and organic mangrove peat horizons, but is instead recorded in bioclastic muddy sand units at 48 cm and 80 cm core depths. Notably, a high-intensity absorption at 1500–1450 cm^{-1}, ascribed to C–H asymmetrical bending in aliphatic CH_3 and scissor bending in aliphatic CH_2, appears in all cores but only at lower than 120 cm relative depth.

Generally, upper mangrove peat at all coring sites is characterized by broad absorption bands at 1640–1582 cm^{-1}, attributed to N–H bending, C=O, aromatic C=C bonds, or asymmetric –COO. Alternatively, peaks around 1660–1630 cm^{-1} can represent C=O stretching in amide groups or the presence of quinone/H–bonded conjugated ketone stretch. Spectra show an increase in aliphatic vibrations (~1500 cm^{-1}) with depth and the emergence of sharp peaks in the range of 1095–1065 cm^{-1} that denote an increase in polysaccharide–related stretches (Stevenson & Goh, 1971; Gaffney et al., 1996; Socrates, 2004; Giovanela et al., 2010) with depth. Notably, TPT-1 did not show vibrations at 1120–1110 cm^{-1} assigned to C–H plane bending and C–C or C–O stretching (Table 2; Figure 5A–B), while this absorption features prominently in the upper 68 cm of TPT-2 and the units underlying coarse sands at TPT-3 (Table 2).

Integration limits (cm^{-1})	Peak name	Assignment	References
1640–1582	1630	N–H bending, C=O, aromatic C=C/ –COO asym (1660–1630 cm^{-1}), C=O stretch in amide groups or quinone/H–bonded conjugated ketone stretch)	*Barreto et al., 2016; Senanayake et al., 2021; Niemeyer et al., 1992; Broder et al., 2012*
1500–1450	1475	CH_2 scissoring alkanes; CH_3 bending asym deformation (aliphatic hydrocarbons)	*Socrates, 2004; Barreto et al., 2016; Obeng et al., 2023*
1170–1150	1160	C–O stretch, esters/ethers/phenols	*Barreto et al., 2016; Obeng et al., 2023*
1120–1100	1110	Si–O–Si stretch (silica); C–H in plane bending, monosubstituted benzenes; C–C or C–OH stretch	*Alahmadi et al. 2012; Socrates, 2004; Gaffney et al., 1996*
1098–1069	1080	Silica; C–O stretch (4 bands), ketals/acetals; C–C or C–OH stretch; C–O polysaccharide stretching	*Krumins et al., 2012; Socrates, 2004; Gaffney et al., 1996*
1060–1054	1060	Silica; C–O polysaccharide stretching (4 bands); ketals/acetals; C–C or C–OH stretch	*Stevenson & Goh, 1971; Gaffney et al., 1996; Giovanela et al., 2010; Broder et al., 2012; Krumins et al; 2012*
1045–1018	1030	Silica; C–O polysaccharide stretching (4 bands); ketals/acetals	*Socrates, 2004; Giovanela et al., 2010; Krumins et al., 2012*
1015–990	1000	Silica (Si–O–Si bending)	*Socrates, 2004*
945–930	940	Silica	*Socrates, 2004*
930–900	915	Silica	*Socrates, 2004*
870–860	865	C–H out–of–plane bending (disubstituted aromatics)	*Pavia et al., 2009*
805–786	790	C–H out–of–plane bending (substituted aromatics); Si–O bending	*Pavia et al., 2009, Yu et al., 2014*
780–765	770	C–H out–of–plane bending (disubstituted aromatics)	*Pavia et al., 2009*
755–740	750	C–H out–of–plane bending (substituted benzene)	*Pavia et al., 2009*
720–705	710	C–H out–of–plane bending (monosubstituted aromatics)	*Pavia et al., 2009*
700–685	690	C–H out–of–plane bending (aromatics, alkenes)	*Socrates, 2004*
670–665	670	C–H out–of–plane bending; C–C bending (substituted aromatics)	*Pavia et al., 2009*
610–595	600	Ring out–of–plane bending; C–Cl bending	*Socrates, 2004; Pavia et al., 2009*
542–516	530	C–X (X = Br, I) bending (halogenated compounds)	*Pavia et al., 2009*
***460–445 (weak)**	450	C–N–C def, secondary amines	*Socrates, 2004*
***470–440 (strong)**	460	Ring in and out–of–plane vibs,/ring out–of–plane def, /C–N–C def, primary amines	*Socrates, 2004*
***440–430 (weak)**	440	C–N–C def, secondary amines	*Socrates, 2004*
***437–416 (strong)**	430	Ring out–of–plane def	*Socrates, 2004*
***425–415 (weak)**	420	C–N–C def, secondary amines	*Socrates, 2004*

Table 1. Summary of absorption bands observed in first and second derivative FT-IR ATR spectra of TPT cores with functional group assignments, peak integration limits by wavenumber (cm^{-1}), and peak name labels.

Core ID	Strat.	Depth (cm)	Wavenumber, cm^{-1}																						
			1640-1582	1500-1450	1170-1150	1120-1100	1098-1069	1060-1054	1045-1018	1015-990	945-930	930-900	870-860	805-786	780-765	755-740	720-705	700-685	670-665	610-595	542-516	***460-445**	***470-440**	***440-430**	***437-416**
TPT-1	Peat	0	*		*				*	*		*		*	*			*			*		*		*
		32	*		*				*	*		*		*	*			*	*		*		*		*
		40	*		*				*	*		*		*	*			*	*		*		*		*
		56	*		*				*	*		*		*	*			*			*		*		*
	F. sand	77			*		*		*	*		*		*	*			*	*		*		*		*
		84			*				*	*		*		*	*			*	*		*		*		*
		128		*	*		*		*	*		*	*	*	*		*	*	*		*		*		*
		184		*	*		*		*	*		*	*	*	*		*	*	*		*		*		
TPT-2	Peat	0	*		*	*			*	*	*	*		*	*			*			*		*		
		20	*		*	*	*		*	*	*	*		*	*			*	*		*		*		*
		36	*		*	*			*	*	*	*		*	*	*		*			*		*		*
		44	*		*	*			*	*	*	*		*	*	*		*			*		*		*
	F. sand	56			*	*	*	*	*	*		*		*	*			*	*		*		*		*
		68			*	*			*	*		*		*	*			*	*		*		*		*
		132		*	*		*		*	*		*	*	*	*		*	*	*		*		*		*
		164		*	*		*		*	*		*	*	*	*		*	*	*		*		*		*
TPT-3	C. sand	0			*		*		*	*		*		*	*			*	*		*		*		*
		16			*			*	*	*		*		*	*			*	*	*	*	*		*	
	Peat	40			*	*	*	*	*	*	*	*		*	*			*	*		*		*		*
	F. sand	48	*		*	*	*	*	*	*	*	*		*	*			*	*	*	*	*	*		*
		60			*		*	*	*	*		*		*	*			*	*		*		*		
		80	*	*	*	*	*		*	*		*		*	*		*	*	*		*	*	*	*	
		120		*	*		*	*	*	*		*		*	*		*	*	*		*	*			
		144		*	*		*	*	*	*		*	*	*	*		*	*	*		*		*		

Table 2. FT-IR absorption bands in 1800–400 cm^{-1} range, of moderate intensity, recorded in representative samples of major stratigraphic units for each TPT core (including mangrove peat, lower fine bioclastic muddy sand, and upper coarse sand). Absorption peaks in the 460–416 cm^{-1} range (starred in bold) represent a single high intensity compound peak centered around 440 cm^{-1} with positions of weaker peaks recorded from observation in second derivative spectra.

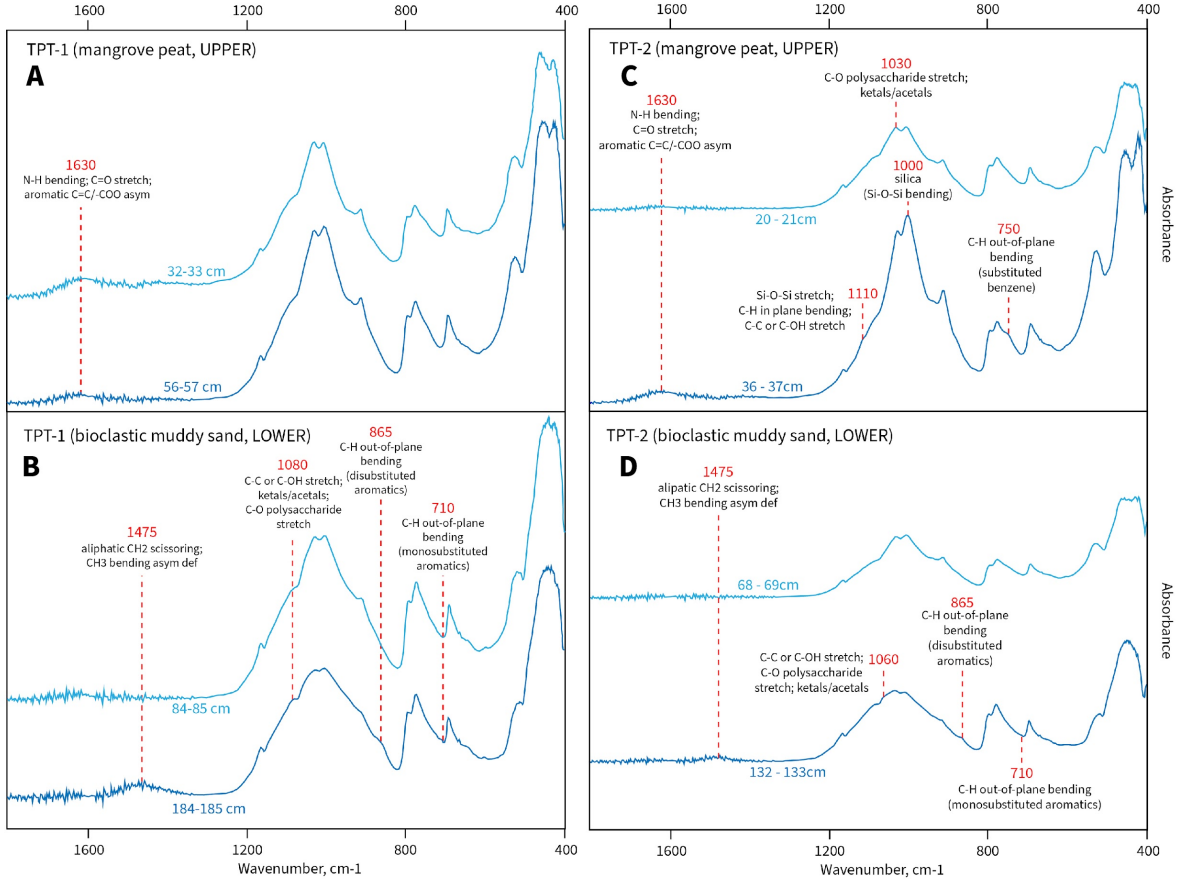

Figure 5. Example FT-IR ATR absorption spectra in the 1800–400 cm^{-1} range for upper mangrove soil units (**A**, **C**) and lower bioclastic muddy sand units (**B**, **D**) in TPT-1 and TPT-2 with characteristics absorptions labeled.

3.6 Humification and decomposition indices

For all TPT cores, the ratio of phenolic moieties to polysaccharide functional groups (I_{1160}/I_{1060}) increases with depth (Figure 6).

TPT-1 shows a relative decrease in humification degree from 0.0552 at the surface (0 cm) to 0.0274 at 56 cm, then a gradual increase to 0.0847 at 184 cm core depth. TPT-2 exhibits a general increase in humification degree with depth with values; ratios range between 0.0283 and 0.0805. TPT-3 mirrors a similar pattern to TPT-1 and TPT-2, showing gradual increase in the ratio of phenolic C–O to polysaccharide C–O intensities with depth.

The humification index, as measured by comparing peak heights at 1630 cm^{-1} (aromatic C=C/–COO stretch) with polysaccharide C–O absorptions at 1060 cm^{-1}, generally decreases with depth for all TPT cores. TPT-1 displays a sharp increase from 0.0690 at 0 cm to 0.1000 at 40 cm depth, then a rapid decrease in I_{1630}/I_{1060} below 40 cm. TPT-2 shows markedly lower ratio values than TPT-1, ranging 0.0330 to 0.0671, but maintaining a similar gradually decreasing pattern with depth. For TPT-3, most ratios measured 0.0000 as peak heights for aromatic moieties could not be determined. Absorption peaks at 1630 cm^{-1} do not appear in the FT-IR spectra for TPT-3 except for samples at 48 cm and 80 cm depth, with respective ratios of 0.0464 and 0.0299, but from limited measurements also appear to decrease with depth overall.

For degree of decomposition (I_{1060}/I_{3300}), TPT-1 displays an increasing trend with depth, from 20.71 at 0 cm to 49.27 at 76 cm, then a sharp depletion in polysaccharide C–O absorption intensity and corresponding increase in O–H alcohol absorption below 128 cm depth where the ratio decreases nearly tenfold to 4.86. Conversely, TPT-2 and TPT-3 showed similar increasing trends of decomposition with depth. TPT-2 ratios range between 35.38 and 64.64, excluding the sample at 68 cm depth where no absorption was recorded for 3300 cm^{-1}. TPT-3 exhibits elevated decomposition ratios, ranging 49.25 to 142.00, and an overall increase with depth.

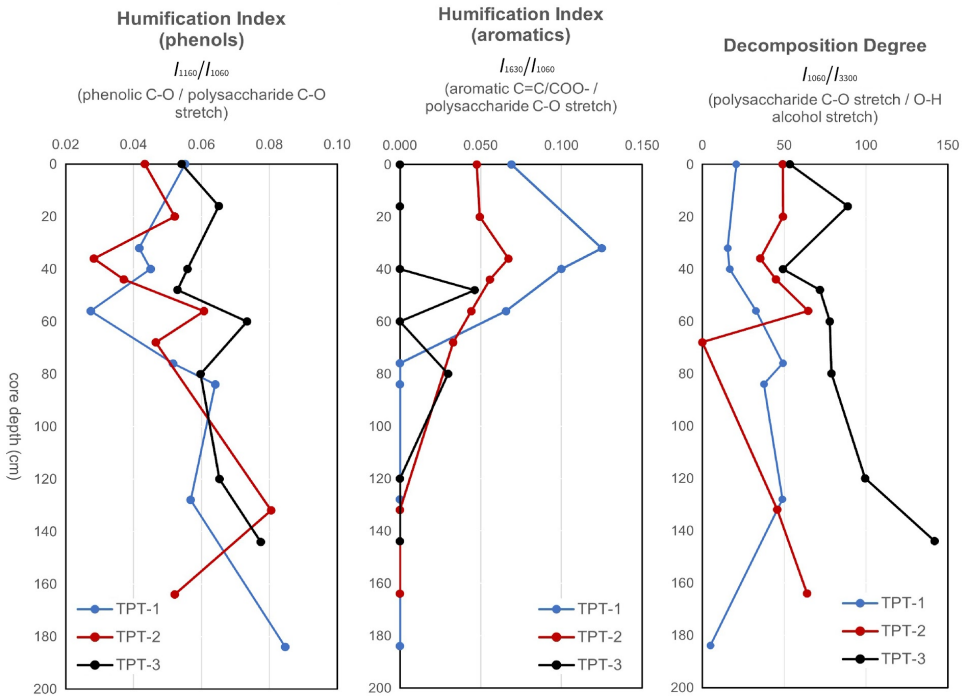

Figure 6. Peak height ratios measured from FT-IR ATR spectra for humification and decomposition degree.

4. Discussion

4.1 Prasae Estuary Mangrove geomorphology

D–GPS mapping (Figure 3) revealed a series of thinly elongated sand ridges segmenting the interior of the PEM forest complex. Mapping demonstrated that mangrove soils formed exclusively on muddy, water–logged substrate in troughed depressions between each sand ridge, consistent with a geomorphological model of a ridge and swale system emerging in response to a gradual sea-level regression during the late Holocene in the Gulf of Thailand (e.g. Somboon, 1988; Sinsakul, 1992; Choowong, 2002; Englong et al., 2019) where a sand ridge develops on the shoreface, similar to the barrier beach currently accreting Prasae River sediments and marine sands at the river mouth, and mangrove plants subsequently colonize the shallowing back-barrier (Ellison, 2019; McLachlan et al., 2020). Organic soil developed in the swale under water–logged conditions by organic matter decomposition and the accumulation of fine sediment delivered by tidal pumping and wave–dominated transport.

4.2 Organic matter source variability and relative inundation changes

OM content ($LOI_{550°C}$ wt%) fluctuations correspond well with positive excursions in TOC/TN measured at the same core depths in all TPT cores, indicating a strong signal for carbon-rich compounds at the mangrove soil surface from leaf litter and other plant–derived inputs to the sediment. Linear regressions for TOC% against TN% suggests similar source origins for carbon–bearing and nitrogenous compounds in all cores.

In general, all TPT cores exhibit a low carbonate content (< 5%) that remains relatively uniform at all depths, consistent with periodic marine tidal inundation. For all TPT cores, carbonate content ($LOI_{950°C}$ wt%) displayed positive excursions when OM content is highest. Elevations in carbonate content with increased soil OM may be linked to enhanced microbial activity in organic-rich horizons from increased decomposition due to higher nutrient availability, leading to a mineralization of organic carbon (Zhou et al., 2019; Tang et al., 2020) that react with calcium ions in the sediment to precipitate carbonate. Water saturation in mangrove sediments tends to generate anoxic conditions, promoting bacterial sulfate reduction and increased soil alkalinity (Krumins et al., 2013; Garcia–Troche et al., 2021), facilitating carbonate precipitation which may also contribute to observed spikes in $LOI_{950°C}$ values.

Loss-on-ignition results closely match observed transitions between stratigraphic units in each core. Mangrove soil, present at all coring sites and covering the modern–day surface at TPT-1 and TPT-2, is characterized geochemically by high organic content (wt%) and TOC/TN values in excess of 20 which strongly points to terrestrial plant–derived contributions to OM (Meyers, 1997) and is consistent with the establishment of dense mangrove forests accumulating leaf litter and active humus formation. OM comprises nearly half of the total sediment mass at the surface of TPT-1 (most inland) and decreases to less than 12% at TPT-3 (most seaward), reflecting the landward increase in mangrove vegetation density which corresponds to amplified primary productivity and leaf litter volume compared to seaward ecological zone. For example, *Ceriops* and *Rhizophora* zones representing the transitional intermediate mangrove in the PEM are defined by heavy canopies of overlapping leaves and entangled stilted root networks that cause trees to grow extremely close together. Conversely, the seaward zone is more exposed and sparsely populated by isolated *Avicennia* and *Sonneratia* trees. Additionally, landward decreases in salinity produce more favorable conditions for plant nutrient uptake which may promote terrestrial plant biodiversity and increase fibrous plant biomass contributions to the soil in the mangrove interior.

The thick unit of muddy sand that underlies mangrove soils in the PEM feature a mixture of immature medium sands punctuated by high energy layers of granule–size fragmentary marine

shells, interpreted to reflect high–energy deposition in a wave–dominated setting such as a beach foreshore or shallow nearshore environment. The bioclastic sand is characterized by distinctively low OM content and TOC/TN below 20 that gradually decreases with depth for all TPT cores. This is consistent with a pattern of increasing decomposition and mineralization with depth.

According to (Meyers, 1997), TOC/TN > 20 indicates terrestrial plant–derived inputs to OM while ratios between 4–10 signify marine contributions from phytoplankton, macroalgae, and aquatic microbial biomass. In TPT-1, the upper 60 cm of mangrove soil displays unusually elevated TOC/TN values between 25–50, highest at the surface then fluctuating by rapidly decreasing with depth to the base of the soil layer. OM is overwhelmingly of plant–derived origin, due to the C-rich nature of mangrove plant lignocellulosic biomass, and relative depletion of TOC with depth suggests active decomposition and organic burial due to microbial breakdown of proteins and the release of nitrogenous compounds. TOC/TN > 25 indicates slower decomposition rates (Andrade et al., 2011; Avramidis and Bekiari, 2021) suggesting a relatively strong presence of undecomposed materials remaining in the mangrove soil or possibly an artifact of continuous leaf litter input to surface sediments from the modern mangrove forest. Below 60 cm, TOC/TN values vacillate between 10–20 with depth to 124 cm, indicating a mixing of terrestrial and aquatic organic sediment inputs which can be interpreted as representing dynamic changes in the inundation regime at TPT-1 as a result of localized sea-level fluctuations through time or variability in freshwater inputs and detrital terrigenous sediments from the Prasae River to the mangrove as accretion occurred. Negative TOC/TN excursions in the bioclastic muddy sands, to less than 10 between 124–148 cm and 164–184 cm, represent at least two recorded periods of marine inundation during higher relative sea-level at the TPT-1 site before a gradual regression to shallow marine or mixed tidal environment and then the strongly terrestrial habitat largely cut off from tidal influence as is present in the PEM today which is consistent with a model of mangrove progradation and landward ecological succession.

TPT-2 displays similar shifts in TOC/TN with depth between upper mangrove soil and lower bioclastic tidal sands, characterized by TOC/TN ratio of nearly 55 at the modern mangrove surface, sharply decreasing with depth to around 20 at the mangrove base, indicative of terrestrial plant–dominated inputs to the soil or dense mangrove cover as well as the active processing and decomposition of leaf litter by microbial and invertebrate communities. Decreasing TOC/TN with depth – 35 at the surface of the underlying sand unit to around 10 at the end of the core – is interpreted to reflect a gradual lowering of relative sea-level through time at TPT-2, although the range of TOC/TN values and fluctuating whole core pattern suggest long periods of dynamic mixing in a transitional setting where contributions to sediment OM may variably include marine, riverine, and vascular plant inputs.

TPT-3 exhibits clear stratification in TOC/TN between the thin surface layer of coarse marine sands, the organic mangrove soil, and the underlying thickness of marine sands. TOC/TN values support an interpretation of a modern seaward mangrove at TPT-3 covered by tidal wash sediments. It appears that OM is actively accumulating at 16–42 cm depth, perhaps preserved from previous forest successions at this locality or arising from modern *in situ* processes, including organic exudates from living mangrove roots that penetrate the sediment or from the decomposition of detrital plant materials and dead roots. There is a strong signal of mixing between terrestrial and aquatic sources of OM in the bioclastic marine sands beneath the mangrove soil, interpreted as the signature for a shallow marine to subaerial transitional environment experiencing dynamic fluctuations in relative sea-level through time as TOC/TN values tend between 10–20. Noticeably, there is evidence of a

sharp positive excursion in TOC/TN at 80 cm depth, consistent with an environmental swing from a mixed input regime to strongly terrestrial increased forest cover. This peak corresponds with only a minor enrichment in organic content (~2% increase from mean OM% at TPT-3) which may suggest a brief period of vascular plant presence at this seaward location in the past, or perhaps a change in local hydrology that may have amplified detrital plant contributions from the Prasae River or increased surface run–off to a shallowing mudflat environment prior to mangrove colonization.

It is difficult to distinguish between marine versus riverine clastic sediment input to the TPT cores from TOC/TN alone, though considering that TPT-3 is situated by an estuarine river mouth in a seaward mangrove zone established on tidal mudflats behind an actively accreting barrier beach, it is assumed that a combination of fluvial and wave–dominated transport processes deliver the majority of allochthonous clastic sediments to the PEM. Tidal pumping effects may also contribute to the apparent landward gradients for humification, decomposition, and TOC/TN observed in the TPT cores. Dense aerial root networks, such as the stilted roots typical of *Rhizophora* trees adapted for intermediate mangrove zones, attenuate tide velocity by increasing drag (Woodroffe et al., 2016; Gijsman et al., 2023) thereby promoting deposition of finer sediment fractions which have been shown to elevate TOC/TN as a result of high surface area increasing OM adsorption to finer–grained particles such as clay minerals, muds, and silts (Li et al., 2024) resulting in increased TOC storage potential inland. In contrast, coarse deposition near the mangrove-shore interface feature characteristically lower TOC/TN reflecting high algal-phytoplankton from daily tidal inundation and a poorer capacity to accumulate OM due to reduced surface area for absorption (Hossain and Bhuiyan, 2016; Li et al., 2024).

4.3 Spectroscopic characterization by FT-IR

For all TPT samples, the weak absorption at 3300 cm^{-1}, potentially corresponding to O–H or N–H stretching, may reflect overlapping contributions from water or proteinaceous material, which require further verification. The peaks at 2925-2905 cm^{-1} correspond to aliphatic C-H stretching, likely derived from waxy plant cuticles or microbial lipids, reinforcing findings from elemental analysis of mixed contributions from both terrestrial and marine sources.

Generally, mangrove soil in the PEM is characterized by absorption peaks at 1630 cm^{-1}, assigned to aromatic C=C and carboxylate ion stretching as well as N–H bending and C=O in amide groups, interpreted as the signal of lignin–derived compounds in mature organic soils arising from humus formation and the enzymatic decomposition of plant lignins into simpler phenolic, and quinone compounds. Observed peaks at 1160 cm^{-1}, corresponding to C-O stretching in phenolic compounds, present in both mangrove organic soils and in the basal sand units of all TPT cores, align well with findings from similar coastal sediments in Senanayake et al. (2021) and lends weight to the important role of lignin catabolism in mangrove soil formation. This signature is consistent with humification theory: cellulosic polysaccharides in fresh leaf litter and detritus are readily decomposed by soil microorganisms (Flores, 2014) while more durable lignin fractions of lignocellulosic biomass are preserved, accumulating in the soil. Subsequent aerobic microbial oxidation converts these lignins into humic substances so highly degraded soils become enriched in carboxylic, aromatic, and phenolic moieties (Norden et al., 1986; Broder et al., 2012).

The distinctive prominence of aromatic compounds in the TPT mangrove soils may not be explained by humification processes alone. For example, Martínez Cortizas et al. (2021) showed FT-IR profiles of *Sphagnum*-peat and fen organic matter displayed relative depletion of phenolic moieties and higher preservation of aliphatic groups instead. Similarly, Broder et al. (2012)

identified low humification rates in *Sphagnum*-peat horizons in ombrotrophic bogs linked to high polyphenol content and high C/N ratios in moss refractory litter. Contrasting findings from other organic sediment studies (e.g. Upton et al, 2018; Vinh et al, 2020) provide compelling evidence that plant litter chemistry exerts strong controls on enzymatic digestion and microbial metabolic pathways (Pradisty et al, 2021), making the type of vegetative contributions to OM a key variable impacting the rate and style of decomposition.

It has been demonstrated experimentally that mangrove leaves contain an abundance of bioactive compounds such as syringyls, p-coumaryls, tannins, vanillic acid, various benzoquinones, flavonoids, and a variety of polyphenols (e.g. Kathiresan and Bingham, 2001; Dahibhate et al., 2018; Audah et al., 2022). Composition and relative proportions may vary between mangrove species, hypothesized in this work to contribute variable chemical signatures to the mangrove soil. However, as FT-IR spectroscopy is a method of elucidating molecular vibrations to identify the presence of functional groups, bulk sediment spectra cannot be used in this context to distinguish the relative contributions of functional moieties without sample spectra of representative plant biomass.

Alternatively, the peak at 1630 cm^{-1} can signify the presence of amide functional groups representing an abundance of nitrogenous compounds in the mangrove sediment, suggestive of an active community of microbial decomposers breaking down plant proteins into smaller peptides (Enggrob et al., 2020) which contribute to a relative enrichment in amide functional groups in mature soils.

TPT-2 mangrove soil uniquely featured peaks at 1110 cm^{-1} (Si–O–Si bending attributed to silica impurities from clastic mineral phases and C–H in plane bending indicating the presence of aromatic rings) and 940 cm^{-1} (assigned to silica) are interpreted to reflect a clastic-rich composition or the presence of clay minerals. Silica and clay inputs to mangrove soil at TPT-2 may be sourced from tidal rivulets and small tributary channels from the Prasae River that feed the PEM interior.

The organic mangrove soil horizon at TPT-3 is very thin compared to TPT-1 and TPT-2, dominated by allochthonous clastics. Although only one representative sample was measured (40 cm), an absorption peak at 1630 cm^{-1} is notably absent from the spectrum. The mangrove soil at TPT-3 displays highly similar spectra to lower bioclastic muddy sands, suggesting inhibited decomposition and microbial activity in the seaward mangrove zone. Elevated TOC in TPT-3 mangrove soil despite lacking aromatic, phenolic, and quinone content in detectable concentrations might alternatively be explained by an accumulation of *in situ* release of organic exudates from living mangrove roots at depth.

An absorption at 670 cm^{-1} is notably absent from the mangrove soil profile at TPT-1 while this vibration is present in all other TPT samples. This difference may point to the appearance of unique peaks in the fingerprint region that can be used to chemically distinguish between mangrove soils from different vegetative zones in future research when compared to reference samples of extant plant matter. It is assumed that there is temporal continuity through the late Holocene in the genera representing ecological zones in the modern mangrove succession.

In contrast, the lower unit of bioclastic muddy sand can be characterized by prominent absorption peaks at 1475 cm^{-1}, linked to CH_2 scissoring alkanes and CH_3 bending asymmetric deformation of aliphatic hydrocarbons potentially derived from plant materials like cuticle waxes or algal lipids. Typically, aliphatic groups display hydrophobic interactions causing close associations with larger grain sizes due to limited OM adsorption and lower solubility in water (Pisani et al., 2014) leading to reduced degradation of aliphatic compounds and preservation in the sedimentary record. There is an abrupt downward shift from 1630 cm^{-1} to 1475 cm^{-1} denoting the transition between mangrove soil and underlying sands for all TPT cores, particularly prominent near the base of each core

(e.g. below 128 cm at TPT-1, below 132 cm at TPT-2, and below 80 cm at TPT-3).

Other characteristic peaks for the lower sand unit include 1080 cm^{-1}, 865 cm^{-1}, and 710 cm^{-1} that appear in all cores, with the addition of silica moieties (940 cm^{-1}) in TPT-2 and TPT-3.

TPT-3 uniquely displays peaks at 450 cm^{-1} and seems to be missing weak absorptions in the 437–416 cm^{-1} range when all other samples from TPT cores feature this absorption, interpreted as a distinguishing geochemical feature between the modern seaward zone and bioclastic sand units for TPT-1 and TPT-2 that were deposited when the shore extent was further inland.

Only TPT-3 featured coarse tidal wash sediments which produced a unique sedimentary finger of weak peaks around 610–595 cm^{-1}, 460–445 cm^{-1}, and 440–430 cm^{-1}. This signal is tentatively interpreted as the influence of riverine sediments in tidal wash or from anthropogenic pollutants due to the presence of C–H out–of–plane bending of various substituted benzene functional groups. This hypothesis required further compound identification techniques to confirm.

4.4 Soil formation processes

Decreasing patterns of humification with depth, as approximated by peak height ratios of recalcitrant lignin–derived phenolic moieties (1110 cm^{-1}) with more labile polysaccharide absorptions (1060 cm^{-1}), for all TPT cores is consistent with a decreasing downward pattern of TOC/TN that signifies burial of decomposed plant litter and subsequent transformation of simpler molecules into phenolic-rich humic substances. I_{1160}/I_{1060} humification index patterns closely mirror relative peak height ratio changes for the degree of decomposition with depth in TPT-2 and TPT-3 while TPT-1 displays a relative depletion of polysaccharide intensities below ~80 cm, interpreted as a lowering of decomposition rate. This contradicts decreasing TOC/TN values below 25 for the lower portion of the TPT-1 core which would suggest a relative acceleration of decomposition rate instead (Andrade et al., 2011).

One explanation for apparent downward suppression of decomposition in TPT-1 involves microbial enzyme inhibition under high phenolic levels, particularly from tannins. An abundance of phenolic compounds in primary leaf litter chemistry or accumulation during humification may dampen decomposition rates (Pradisty et al., 2021; Kim et al., 2021) and create negative feedback that improve aliphatic hydrocarbon preservation at depth.

Sulfur reduction is widely reported as a key metabolic pathway in marine and mangrove sediments (e.g. Sherman et al., 1998; Alongi, 2005; Kumar et al., 2018; Li et al., 2021; Kashif et al., 2023). Anaerobic conditions in water–logged sediments are favorable to sulfur–reducing bacteria that utilize sulfate as electron acceptors, a process that promotes OM decomposition (Nagakura et al., 2022; Laux et al., 2024). However, the production of inhibitory compounds such as hydrogen sulfide and other reduced sulfur species creates toxicity for decomposer communities that may result in a slowing down of humification and decomposition processes at depth (Mo et al., 2023; Laux et al., 2024). It is possible that sulfur–reducing pathways in the anoxic, isolated nature of the deeper sands underlying a more terrestrial intermediate mangrove setting at TPT-1, less affected by bioturbation and mixed inputs from daily inundation at the surface, could account for an apparent reduction in decomposition degree with depth at this locality. Further verification is required to resolve this hypothesis.

5. Conclusions

This study examined how the chemical characterization of bulk organic mangrove sediment (e.g. LOI, TOC/TN, and functional group assemblages determined by FT-IR spectra) is associated with lithostratigraphic variability and sediment input shifts in response to environmental changes in sea-level, inundation regime, and terrestrial freshwater inputs:

- LOI and elemental analyses showed obvious excursions that denote sharp boundaries between sedimentary units in the PEM, categorized into nutrient–poor surface tidal wash sediments, organic-rich upper mangrove soils with active humus formation, and underlying bioclastic sands low in organic content.
- LOI and elemental analyses support higher rates of organic decomposition in oxygenated, bioturbated surface sediments of immature mangrove soils.
- TOC/TN values and geomorphic evidence supports an interpretation of dynamic relative sea-level change and variable inundation regimes, reflected in relative shifts in the dominant source of sediment OM.
- High overall TOC/TN values in all cores suggests predominantly allochthonous terrestrial plant inputs to organic sediment in the PEM, likely from two main sources: 1) the direct decomposition or mangrove leaf litter and humification during organic soil formation, and 2) detrital organic matter from terrestrial sources via run–off and riverine sediments delivered from the nearby Prasae River mouth.
- Inferred detrital terrigenous input from direct surface run–off and riverine sediment may have increased during wetter conditions of late Holocene in eastern Thailand.
- TOC/TN values between 10–20 recorded for much of the basal sands (bioclastic muddy sand) show strong mixing signal and OM source variability, interpreted to reflect transitions between rising and falling relative sea-level.
- FT-IR ATR can be used to chemically distinguish between different sedimentary units and profile differences in the fingerprint region has the potential to discriminate signatures of different mangrove vegetative zones.
- Organic mangrove soil in the PEM is enriched in phenolic, aromatic, and quinone functional groups denoted by an obvious peak at 1630 cm^{-1}.
- Basal sands in the PEM are characterized by preservation of aliphatic hydrocarbon groups, marked by a peak at 1475 cm^{-1}.

Acknowledgements

We thank the Department of Marine and Coastal Resources and the Subdistrict Municipality of Pak Nam Prasae for permission to collect samples. We thank the Department of Chemistry at Chulalongkorn University, for access to spectroscopic instrumentation. We thank Assoc. Prof. Dr Pei-Ling Wang and her team of specialists at the Institute of Oceanography, National Taiwan University (IONTU) for the generous use of facilities for elemental analysis. We especially thank Dr Smith Leknettip for their generous support and constructive feedback, as well as members of the Department of Geology at Chulalongkorn University for assistance during field work.

References

Alahmadi, S.M., Mohamad, S., Maah, M.J., 2012. Synthesis and Characterization of Mesoporous Silica Functionalized with Calix [] arene Derivatives. International Journal of Molecular Sciences 13, 13726–13736.

Alogi, D.M., 2020. Global Significance of Mangrove Blue Carbon in Climate Change Mitigation. Sci 2, 67. Alongi, D.M., 2018. Impact of Global Change on Nutrient Dynamics in Mangrove Forests. Forests 9, 596.

Alongi, D.M., 2014. Carbon Cycling and Storage in Mangrove Forests. Annual Review of Marine Science 6, 195–219.

Alongi, D.M., 2005. Mangrove–Microbe–Soil Relations, in: Interactions Between Macro– and Microorganisms in Marine Sediments. American Geophysical Union (AGU), pp. 85–103.

Andrade, A., Rubio, B., Rey, D., Álvarez–Iglesias, P., Bernabeu, A.M., Vilas, F., 2011. Palaeoclimatic changes in the NW Iberian

-Peninsula during the last 3000 years inferred from -diagenetic -proxies in the Ría de Muros sedimentary record. Climate Research 48, 247–259.
Audah, K.A., Ettin, J., Darmadi, J., Azizah, N.N., Anisa, A.S., Hermawan, T.D.F., Tjampakasari, C.R., Heryanto, R., Ismail, I.S., Batubara, I., 2022. Indonesian Mangrove Sonneratia caseolaris Leaves Ethanol Extract Is a Potential Super Antioxidant and Anti Methicillin–Resistant Staphylococcus aureus Drug. Molecules 27, 8369.
Avramidis, P., Bekiari, V., 2021. Application of a catalytic oxidation method for the simultaneous determination of total organic carbon and total nitrogen in marine sediments and soils. PLOS ONE 16, e0252308.
Ballian, A., Chawchai, S., Miocic, J.M., Charoenchatree, W., Bissen, R., Preusser, F., 2024. Late Holocene coastal dynamics south of the Chanthaburi estuary, eastern Gulf of Thailand. Quaternary Research 117, 19–29.
Barreto, M.B., Lo Mónaco, S., Díaz, R., Barreto–Pittol, E., López, L., Peralba, M. do C.R., 2016. Soil organic carbon of mangrove forests (Rhizophora and Avicennia) of the Venezuelan Caribbean coast. Organic Geochemistry 100, 51–61.
Beck, H.E., Zimmermann, N.E., McVicar, T.R., Vergopolan, N., Berg, A., Wood, E.F., 2018. Present and future Köppen–Geiger climate classification maps at 1–km resolution. Sci Data 5, 180214.
Bianchi, T.S., Canuel, E.A., 2011. Chemical Biomarkers in Aquatic Ecosystems. Princeton University Press.
Broder, T., Blodau, C., Biester, H., Knorr, K.H., 2012. Peat decomposition records in three pristine ombrotrophic bogs in southern Patagonia. Biogeosciences 9, 1479–1491.
Carneiro, L.M., do Rosário Zucchi, M., de Jesus, T.B., da Silva Júnior, J.B., Hadlich, G.M., 2021. δ13C, δ15N and TOC/TN as indicators of the origin of organic matter in sediment samples from the estuary of a tropical river. Marine Pollution Bulletin 172, 112857.
Chabangborn, A., 2017. Review of Paleoclimatic Reconstruction in Thailand Between the Last Glacial Maximum and the Mid Holocene. Burapha Science Journal 61–77.
Chmura, G.L., Anisfeld, S.C., Cahoon, D.R., Lynch, J.C., 2003. Global carbon sequestration in tidal, saline wetland soils. Global Biogeochemical Cycles 17.
Choowong, M., n.d. Lithofacies and episodic coastal evolution from the Eastern part of Thailand 7.
Dahibhate, N.L., Saddhe, A.A., Kumar, K., 2019. Mangrove Plants as a Source of Bioactive Compounds: A Review. The Natural Products Journal 9, 86–97.
Duarte, C.M., Middelburg, J.J., Caraco, N., 2005. Major role of marine vegetation on the oceanic carbon cycle. Biogeosciences 2, 1–8.
Ellison, J.C., 2019. Chapter 20 – Biogeomorphology of Mangroves, in: Perillo, G.M.E., Wolanski, E., Cahoon, D.R., Hopkinson, C.S. (Eds.), Coastal Wetlands (Second Edition). Elsevier, pp. 687–715.
Enggrob, K.L., Larsen, T., Peixoto, L., Rasmussen, J., 2020. Gram–positive bacteria control the rapid anabolism of protein–sized soil organic nitrogen compounds questioning the present paradigm. Sci Rep 10, 15840.
Englong, A., Punwong, P., Selby, K., Marchant, R., Traiperm, P., Pumijumnong, N., 2019. Mangrove dynamics and environmental changes on Koh Chang, Thailand during the last millennium. Quaternary International, SI: Quaternary International 500 500, 128–138.
Fenchel, T., King, G.M., Blackburn, T.H., 2012. Chapter 3 – Degradation of Organic Polymers and Hydrocarbons, in: Fenchel, T., King, G.M., Blackburn, T.H. (Eds.), Bacterial Biogeochemistry (Third Edition). Academic Press, Boston, pp. 49–57.
Flores, R.M., 2014. Chapter 3 – Origin of Coal as Gas Source and Reservoir Rocks, in: Flores, R.M. (Ed.), Coal and Coalbed Gas. Elsevier, Boston, pp. 97–165.
Gaffney, J.S., Marley, N.A., Clark, S.B., 1996. Humic and Fulvic Acids and Organic Colloidal Materials in the Environment, in: Humic and Fulvic Acids, ACS Symposium Series. American Chemical Society, pp. 2–16.
García–Troche, E.M., Morell, J.M., Meléndez, M., Salisbury, J.E., 2021. Carbonate chemistry seasonality in a tropical mangrove lagoon in La Parguera, Puerto Rico. PLOS ONE 16, e0250069.
Gijsman, R., Horstman, E.M., Swales, A., MacDonald, I.T., Bouma, T.J., van der Wal, D., Wijnberg, K.M., 2024. Mangrove forest drag and bed stabilisation effects on intertidal flat morphology. Earth Surface Processes and Landforms 49, 1117–1134.
Giovanela, M., Crespo, J.S., Antunes, M., Adamatti, D.S., Fernandes, A.N., Barison, A., da Silva, C.W.P., Guégan, R., Motelica–Heino, M., Sierra, M.M.D., 2010. Chemical and spectroscopic characterization of humic acids

extracted from the bottom sediments of a Brazilian subtropical microbasin. Journal of Molecular Structure 981, 111–119.
González–Pérez, M., Vidal Torrado, P., Colnago, L.A., Martin–Neto, L., Otero, X.L., Milori, D.M.B.P., Gomes, F.H., 2008. 13C NMR and FTIR spectroscopy characterization of humic acids in spodosols under tropical rain forest in southeastern Brazil. Geoderma 146, 425–433.
Google Earth, 2022. Prasae Estuary and Thung Prong Thong Mangrove Complex, 1:150,000 [WWW Document]. Google Earth.
Hayes, M.H.B., Swift, R.S., 2020. Chapter 1 – Vindication of humic substances as a key component of organic matter in soil and water, in: Sparks, D.L. (Ed.), Advances in Agronomy. Academic Press, pp. 1–37.
Hossain, G.M., Bhuiyan, M.A.H., 2016. Spatial and temporal variations of organic matter contents and potential sediment nutrient index in the Sundarbans mangrove forest, Bangladesh. KSCE J Civ Eng 20, 163–174.
Hossain, M.D., Nuruddin, A.A., 2016. Soil and Mangrove: A Review. Journal of Environmental Science and Technology 9, 198–207.
Jia, M., Wang, Z., Mao, D., Ren, C., Song, K., Zhao, C., Wang, C., Xiao, X., Wang, Y., 2023. Mapping global distribution of mangrove forests at 10–m resolution. Science Bulletin 68, 1306–1316. https://doi.org/10.1016/j.scib.2023.05.004
Kashif, M., Sang, Y., Mo, S., Rehman, S. ur, Khan, S., Khan, M.R., He, S., Jiang, C., 2023. Deciphering the biodesulfurization pathway employing marine mangrove Bacillus aryabhattai strain NM1–A2 according to whole genome sequencing and transcriptome analyses. Genomics 115, 110635.
Kathiresan, K., Bingham, B.L., 2001. Biology of mangroves and mangrove ecosystems. Advances in Marine Biology 40, 81–251.
Kim, J., Lee, J., Yang, Y., Yun, J., Ding, W., Yuan, J., Khim, J.S., Kwon, B.–O., Kang, H., 2021. Microbial decomposition of soil organic matter determined by edaphic characteristics of mangrove forests in East Asia. Science of The Total Environment 763, 142972.
Krumins, J., Klavins, M., Seglins, V., Kaup, E., 2012. Comparative Study of Peat Composition by using FT-IR Spectroscopy. Materialzinatne un Lietiska Kimija 26, 106.
Krumins, V., Gehlen, M., Arndt, S., Van Cappellen, P., Regnier, P., 2013. Dissolved inorganic carbon and alkalinity fluxes from coastal marine sediments: model estimates for different shelf environments and sensitivity to global change. Biogeosciences 10, 371–398.
Kumar, U., Panneerselvam, P., Gupta, V.V.S.R., Manjunath, M., Priyadarshinee, P., Sahoo, A., Dash, S.R., Kaviraj, M., Annapurna, K., 2018. Diversity of Sulfur–Oxidizing and Sulfur–Reducing Microbes in Diverse Ecosystems, in: Adhya, T.K., Lal, B., Mohapatra, B., Paul, D., Das, S. (Eds.), Advances in Soil Microbiology: Recent Trends and Future Prospects: Volume 1: Soil–Microbe Interaction. Springer, Singapore, pp. 65–89.
Laux, M., Ciapina, L.P., de Carvalho, F.M., Gerber, A.L., Guimarães, A.P.C., Apolinário, M., Paes, J.E.S., Jonck, C.R., de Vasconcelos, A.T.R., 2024. Living in mangroves: a syntrophic scenario unveiling a resourceful microbiome. BMC Microbiol 24, 228.
Li, M., Fang, A., Yu, X., Zhang, K., He, Z., Wang, C., Peng, Y., Xiao, F., Yang, T., Zhang, W., Zheng, X., Zhong, Q., Liu, X., Yan, Q., 2021. Microbially–driven sulfur cycling microbial communities in different mangrove sediments. Chemosphere 273, 128597.
Li, Y., Long, C., Dai, Z., Zhou, X., 2024. Pattern of total organic carbon in sediments within the mangrove ecosystem. Front. Mar. Sci. 11.
Madumini Senanayake, N.D., Ratnayake, A.S., Premila Wijesinghe, U.M., Ratnayake, N.P., 2021. Geochemistry and sedimentology of tropical mangrove sediments along the southwest coast of Sri Lanka: Fingerprints for development history of wetlands. Regional Studies in Marine Science 46, 101884.
Martínez Cortizas, A., Sjöström, J.K., Ryberg, E.E., Kylander, M.E., Kaal, J., López-Costas, O., Álvarez Fernández, N., Bindler, R., 2021. 9000 years of changes in peat organic matter composition in Store Mosse (Sweden) traced using FTIR-ATR. Boreas 50, 1161–1178.
Mathew, J., Gopinath, A., Vareed, R.A., 2021. Spectroscopic characterization of humic substances isolated from tropical mangrove sediments. Arab J Geosci 14, 668.
McLachlan, R.L., Ogston, A.S., Asp, N.E., Fricke, A.T., Nittrouer, C.A., Schettini, C.A.F., 2020. Morphological evolution of a macrotidal back-barrier environment: The Amazon Coast. Sedimentology 67, 3492–3512.
Mcleod, E., Chmura, G.L., Bouillon, S., Salm, R., Björk, M., Duarte, C.M., Lovelock, C.E., Schlesinger, W.H., Silliman, B.R., 2011. A blueprint for blue carbon: toward an improved understanding of the role of vegetated coastal habitats in sequestering CO2. Frontiers in Ecology and the Environment 9, 552–560.

Meyers, P.A., 1997. Organic geochemical proxies of paleoceanographic, paleolimnologic, and paleoclimatic processes. Organic Geochemistry 27, 213–250.
Miocic, J.M., Sah, R., Chawchai, S., Surakiatchai, P., Choowong, M., Preusser, F., 2022. High resolution luminescence chronology of coastal dune deposits near Chumphon, Western Gulf of Thailand. Aeolian Research 56, 100797.
Mo, S., Yan, B., Gao, T., Li, J., Kashif, M., Song, J., Bai, L., Yu, D., Liao, J., Jiang, C., 2023. Sulfur metabolism in subtropical marine mangrove sediments fundamentally differs from other habitats as revealed by SMDB. Sci Rep 13, 8126.
Nagakura, T., Schubert, F., Wagner, D., Kallmeyer, J., IODP Exp. 385 Shipboard Scientific Party, 2022. Biological Sulfate Reduction in Deep Subseafloor Sediment of Guaymas Basin. Front. Microbiol. 13.
Nardi, S., Schiavon, M., Francioso, O., 2021. Chemical Structure and Biological Activity of Humic Substances Define Their Role as Plant Growth Promoters. Molecules 26, 2256.
Niemeyer, J., Chen, Y., Bollag, J.–M., 1992. Characterization of Humic Acids, Composts, and Peat by Diffuse Reflectance Fourier-Transform Infrared Spectroscopy. Soil Science Society of America Journal 56, 135–140.
Norden, B., Fyfe, C.A., McKinnon, M.S., 1986. 13C CP/MAS NMR study of peat in the solid state. International Peat Journal 1, 153–164.
Obeng, A.S., Dunne, J., Giltrap, M., Tian, F., 2023. Soil organic matter carbon chemistry signatures, hydrophobicity and humification index following land use change in temperate peat soils. Heliyon 9.
Pavia, D.L., Lampman, G.M., Kriz, G.S., Vyvyan, J.R., 2009. Introduction to Spectroscopy, 4th ed. Brooks/Cole, USA.
Pernetta, J., 1993. Mangrove Forests, Climate Change and Sea Level Rise: Hydrological Influences on Community Structure and Survival, with Examples from the Indo–West Pacific. IUCN.
Pisani, O., Hills, K.M., Courtier–Murias, D., Haddix, M.L., Paul, E.A., Conant, R.T., Simpson, A.J., Arhonditsis, G.B., Simpson, M.J., 2014. Accumulation of aliphatic compounds in soil with increasing mean annual temperature. Organic Geochemistry 76, 118–127.
Pradisty, N.A., Amir, A.A., Zimmer, M., 2021. Plant species– and stage–specific differences in microbial decay of mangrove leaf litter: the older the better? Oecologia 195, 843–858.
Scholl, D.W., 1997. Mangrove swamps: geology and sedimentology Mangrove swamps: Geology and sedimentology, in: Geomorphology. Springer, Berlin, Heidelberg, pp. 683–688. https://doi.org/10.1007/3–540–31060–6_237
Sherman, R.E., Fahey, T.J., Howarth, R.W., 1998. Soil–plant interactions in a neotropical mangrove forest: iron, phosphorus and sulfur dynamics. Oecologia 115, 553–563. https://doi.org/10.1007/s004420050553
Shiau, Y.–J., Chiu, C.–Y., 2020. Biogeochemical Processes of C and N in the Soil of Mangrove Forest Ecosystems. Forests 11, 492.
Sinsakul, S., 1992. Evidence of Quaternary sea level changes in the coastal areas of Thailand: a review. Journal of Southeast Asian Earth Sciences, Global Environmental Change the Role of the Geoscientist Past, Present and Future Sea-level changes 7, 23–37.
Slatt, R.M., 2013. Chapter 10 – Nondeltaic, Shallow Marine Deposits and Reservoirs, in: Slatt, R.M. (Ed.), Developments in Petroleum Science, Stratigraphic Reservoir Characterization for Petroleum Geologists, Geophysicists, and Engineers. Elsevier, pp. 441–473.
Socrates, G., 2004. Infrared and Raman Characteristic Group Frequencies: Tables and Charts. John Wiley & Sons.
Somboon, J.R.P., 1988. Paleontological study of the recent marine sediments in the lower central plain, Thailand. Journal of Southeast Asian Earth Sciences 2, 201–210.
Stevenson, F.J., Goh, K.M., 1971. Infrared spectra of humic acids and related substances. Geochimica et Cosmochimica Acta 35, 471–483.
Tang, C.–S., Yin, L., Jiang, N., Zhu, C., Zeng, H., Li, H., Shi, B., 2020. Factors affecting the performance of microbial–induced carbonate precipitation (MICP) treated soil: a review. Environ Earth Sci 79, 94.
Twilley, R., Day, J., 2012. Estuarine Ecology, Second Edition. pp. 165–202.
Twilley, R.R., Chen, R.H., Hargis, T., 1992. Carbon sinks in mangroves and their implications to carbon budget of tropical coastal ecosystems. Water Air Soil Pollut 64, 265–288.
Upton, A., Vane, C.H., Girkin, N., Turner, B.L., Sjögersten, S., 2018. Does litter input determine carbon storage and peat organic chemistry in tropical peatlands? Geoderma 326, 76–87.
Vinh, T.V., Allenbach, M., Linh, K.T.V., Marchand, C., 2020. Changes in Leaf Litter Quality During Its Decomposition in a Tropical Planted

Mangrove Forest (Can Gio, Vietnam). Frontiers in Environmental Science 8.
Woodroffe, C.D., 2018. Mangrove response to sea level rise: palaeoecological insights from macrotidal systems in northern Australia. Mar. Freshwater Res. 69, 917–932.
Woodroffe, C.D., 1992. Mangrove sediments and geomorphology, in: Tropical Mangrove Ecosystems, Coastal and Estuarine Studies. American Geophysical Union (AGU), pp. 7–42.
Woodroffe, C.D., Rogers, K., McKee, K.L., Lovelock, C.E., Mendelssohn, I.A., Saintilan, N., 2016. Mangrove Sedimentation and Response to Relative Sea-level Rise. Annual Review of Marine Science 8, 243–266.
Worthington, T.A., zu Ermgassen, P.S.E., Friess, D.A., Krauss, K.W., Lovelock, C.E., Thorley, J., Tingey, R., Woodroffe, C.D., Bunting, P., Cormier, N., Lagomasino, D., Lucas, R., Murray, N.J., Sutherland, W.J., Spalding, M., 2020. A global biophysical typology of mangroves and its relevance for ecosystem structure and deforestation. Sci Rep 10, 14652.
Yulianto, E., Sukapti, W.S., Rahardjo, A.T., Noeradi, D., Siregar, D.A., Suparan, P., Hirakawa, K., 2004. Mangrove shoreline responses to Holocene environmental change, Makassar Strait, Indonesia. Review of Palaeobotany and Palynology 131, 251–268.
Zhang, Y., Du, J., Zhang, F., Yu, Y., Zhang, J., 2011. Chemical characterization of humic substances isolated from mangrove swamp sediments: The Qinglan area of Hainan Island, China. Estuarine, Coastal and Shelf Science, Dynamics of Chinese Muddy Coasts and Estuaries 93, 220–227.
Zhou, W., Han, G., Liu, M., Li, X., 2019. Effects of soil pH and texture on soil carbon and nitrogen in soil profiles under different land uses in Mun River Basin, Northeast Thailand. PeerJ 7, e7880.
Zhu, J.–J., Yan, B., 2022. Blue carbon sink function and carbon neutrality potential of mangroves. Science of The Total Environment 822, 153438.